Cardiac and vascular functions of the zebrafish orthologues of the type I neurofibromatosis gene *NF1*

Arun Padmanabhan[a,1], Jeong-Soo Lee[b,1], Fraz A. Ismat[c], Min Min Lu[a], Nathan D. Lawson[d], John P. Kanki[b], A. Thomas Look[b,2], and Jonathan A. Epstein[a,2]

[a]Department of Cell and Developmental Biology, Penn Cardiovascular Institute, and the Institute for Regenerative Medicine, University of Pennsylvania, Philadelphia, PA 19104; [b]Department of Pediatric Oncology, Dana-Farber Cancer Institute, Harvard Medical School, Boston, MA 02115; [c]Division of Cardiology, Department of Pediatrics, Children's Hospital of Philadelphia, Philadelphia, PA 19104; and [d]Program in Gene Function and Expression, University of Massachusetts Medical School, Worcester, MA 06105

Edited by Eric N. Olson, University of Texas Southwestern Medical Center, Dallas, TX, and approved October 14, 2009 (received for review February 20, 2009)

Von Recklinghausen neurofibromatosis is a common autosomal dominant genetic disorder characterized by benign and malignant tumors of neural crest origin. Significant progress in understanding the pathophysiology of this disease has occurred in recent years, largely aided by the development of relevant animal models. Von Recklinghausen neurofibromatosis is caused by mutations in the *NF1* gene, which encodes neurofibromin, a large protein that modulates the activity of Ras. Here, we describe the identification and characterization of zebrafish *nf1a* and *nf1b*, orthologues of *NF1*, and show neural crest and cardiovascular defects resulting from morpholino knockdown, including vascular and cardiac valvular abnormalities. Development of a zebrafish model of von Recklinghausen neurofibromatosis will allow for structure-function analysis and genetic screens in this tractable vertebrate system.

cardiovascular | neurofibromin

Von Recklinghausen neurofibromatosis (NF1) is caused by mutations in the *NF1* gene that result in a wide variety of symptoms expressed with variable penetrance among affected individuals (1). NF1 patients inherit a single mutated copy of *NF1* and may acquire additional somatic mutations in the wild-type allele that contribute to disease progression (2). Cutaneous neurofibromas, benign Schwann-cell tumors derived from the neural crest, are a pathogneumonic lesion of this disease and often appear in large numbers. More serious oncogenic lesions, including neurofibrosarcomas and malignant peripheral nerve sheath tumors, may also develop. Additional neural crest-related pathologies include pheochromocytomas and hyperpigmented lesions arising from melanocyte abnormalities known as café-au-lait spots. Non-neural-crest-related abnormalities are also common and include cognitive and learning deficits, skeletal abnormalities, and leukemia. Affected individuals also display an increased incidence of cardiovascular pathologies, including hypertension, renal artery stenosis, and congenital heart disease (3).

Neurofibromin, the product of the *NF1* gene, is a protein of >2,800 aa. It contains a small region homologous to yeast IRA proteins that includes a Ras-GTPase-activating domain (GAP) capable of accelerating the hydrolysis of GTP-bound Ras, thus down-regulating the activity of Ras proto-oncogenes (4). Though additional extensive regions of neurofibromin have been conserved across evolution, other functions of this protein are largely unknown. Evidence from analysis of the Drosophila *NF1* orthologue (5, 6) and mouse models of NF1 (7, 8) implicate a role for neurofibromin in modulating cAMP-dependent protein kinase A signaling. Unrelated work suggests that neurofibromin can associate with microtubules (9) as well as other molecules able to induce cytoskeletal changes (10).

The past 15 years have seen the emergence of increasingly sophisticated mouse models of NF1 (11–23). Genetic inactivation of murine *Nf1* results in midgestation embryonic lethality with deficient embryos displaying congenital heart disease involving the cardiac outflow tract and endocardial cushions. Heterozygous *Nf1*-deficient mice are viable and fertile, exhibit learning defects (24, 25), and develop malignancies, albeit at a low rate over a period of several years. Genetic inactivation of the *p53* tumor suppressor gene augments the disease phenotype in mouse models of NF1 and leads to a dramatic increase in the rate of malignancy (14, 15, 26, 27).

Tissue-specific *Nf1* gene inactivation using Cre-lox technology has led to the development of mouse models that more accurately reproduce aspects of the human disease. For example, Schwann cell-specific inactivation of *Nf1* results in the development of malignant peripheral nerve sheath tumors in all animals (19, 28). *Nf1* inactivation in the developing neural crest using Pax3- or Wnt1-Cre results uniformly in early neonatal lethality, with affected animals exhibiting massive overgrowths of peripheral nervous tissue, including the dorsal root and sympathetic ganglia (11, 20). Related investigations have implicated a role for the heterozygous tumor microenvironment as a major contributor to the development of disease (19, 28). Tissue-specific inactivation studies have also identified a critical role for neurofibromin in endothelial cells as Tie2-Cre-mediated *Nf1* inactivation reproduces the cardiac abnormalities associated with the $Nf1^{-/-}$ phenotype (11, 20). *Nf1* inactivation in blood leads to the development of juvenile myelomonocytic leukemia (JMML), the specific form of leukemia found in NF1 patients (29–31). *Nf1* function in mast cells and neurofibromin-mediated modulation of Ras/Erk signaling downstream of c-Kit have also been implicated in tumor progression (32).

Though mouse and Drosophila models of NF1 have proven to be informative, additional information will be obtained from alternative model systems. In particular, vertebrate models that allow for high-throughput in vivo screens and rapid, cost-effective phenotypic analysis may facilitate discovery of novel functions and therapeutic approaches. Hence, we sought to develop a zebrafish model of NF1 and to use this model system to elucidate novel developmental functions of neurofibromin. Here, we describe two closely related zebrafish orthologues: *nf1a* and *nf1b*. Transient knockdown of either gene, or both together, during embryogenesis results in developmental defects of cardiac and neural crest structures that closely resemble murine models and aspects of the human disease. In addition, we identify

Author contributions: A.P., F.A.I., N.D.L., J.P.K., A.T.L., and J.A.E. designed research; A.P., J.-S.L., F.A.I., and M.M.L. performed research; J.-S.L. and N.D.L. contributed new reagents/analytic tools; A.P., F.A.I., and J.A.E. analyzed data; and A.P. and J.A.E. wrote the paper.

The authors declare no conflict of interest.

This article is a PNAS Direct Submission.

[1]A.P. and J.-S.L. contributed equally to this work.

[2]To whom correspondence may be addressed at: 1154 BRB II/III, 421 Curie Boulevard, Philadelphia, PA 19104 or Mayer Building, Room 630, 44 Binney Street, Boston, MA 02115. E-mail: epsteinj@mail.med.upenn.edu or thomas_look@dfci.harvard.edu.

This article contains supporting information online at www.pnas.org/cgi/content/full/0901932106/DCSupplemental.

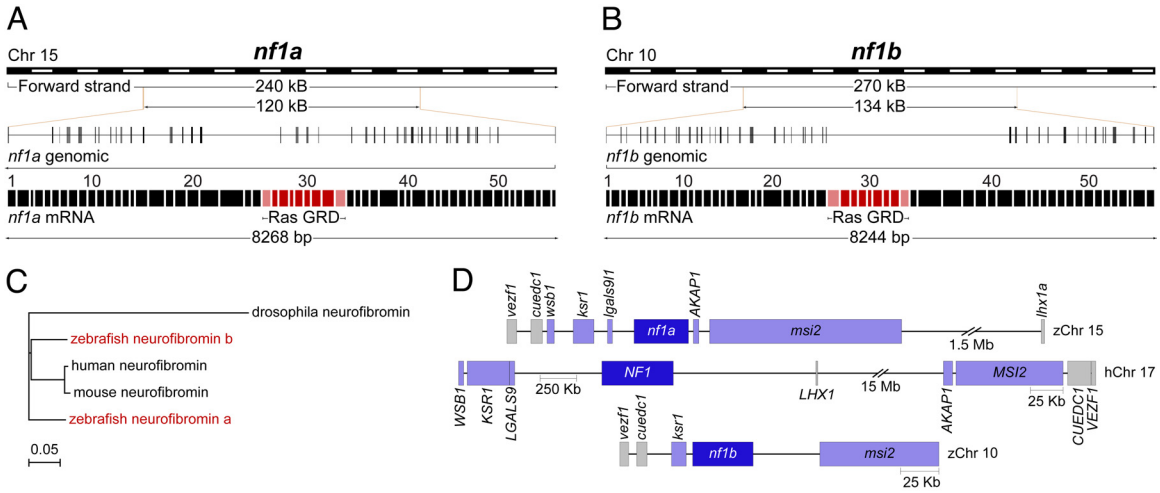

Fig. 1. Zebrafish have two orthologues of human *NF1*. (*A* and *B*) Genomic and mRNA structures of the two orthologous zebrafish genes corresponding to human *NF1*. (*C*) Phylogenetic tree comparison of zebrafish, human, mouse, and Drosophila neurofibromin. (*D*) Analysis of syntenic relationships between human chromosome 17 (*NF1*) and zebrafish chromosomes 15 (*nf1a*) and 10 (*nf1b*). Relative genomic positions are to scale as indicated.

a previously unrecognized vascular defect apparent in zebrafish and mice.

Results

Identification of *nf1a* and *nf1b*. We used a bioinformatics approach to identify the zebrafish orthologues of human *NF1*. Analysis of the eighth assembly (Zv8) of the zebrafish genome revealed two genes highly similar to *NF1* at the amino acid level (90.4% and 90.7%, respectively), which we named *nf1a* and *nf1b*. These genes are highly related to one another (87.4% identical and 93.7% similar), with *nf1a* and *nf1b* sharing similar genomic structures and each containing 57 exons (Fig. 1 *A* and *B*). *nf1a* is located on chromosome 15 (Fig. 1*A*) and predicts a 311-kDa protein composed of 2,755 aa, whereas *nf1b* is located on chromosome 10 (Fig. 1*B*) and predicts a 310-kDa protein composed of 2,747 aa.

Comparison to Drosophila, murine, and human neurofibromin protein sequences reveals significant conservation in the GAP and IRA homology domains and also in extensive areas flanking these regions, suggesting additional functional motifs that have been conserved across evolution (Fig. S1). A phylogenetic tree (Fig. 1*C*) shows a tight clustering of the zebrafish neurofibromin orthologues with other mammalian neurofibromins and a divergence from the Drosophila neurofibromin orthologue. Human/zebrafish synteny maps and bioinformatics analyses suggest that *nf1a* and *nf1b* likely arose via gene duplication (Fig. 1*D*). Upstream of the human *NF1* gene on chromosome 17 are genes encoding WD repeat and SOCS box-containing 1 (*WSB1*), kinase suppressor of Ras 1 (*KSR1*), and Galectin-9 (*LGALS9*), whereas A kinase anchor protein 1 (*AKAP1*) and RNA-binding protein Musashi homolog 2 (*MSI2*) both lie downstream of *NF1*. Similar genes flank *nf1a*, whereas *nf1b* is flanked only by orthologues of *KSR1* and *MSI2*. The identification of duplicated genes is common in zebrafish and reflects the well-described chromosomal doubling event occurring early in teleost evolution (33).

The GenBank EST database identified expressed sequence tags for both zebrafish *nf1* genes in many tissues, including the heart (Fig. S2*A* and Tables S1 and S2), suggesting that neither gene is likely to be a pseudogene and that they are expressed in overlapping tissues. We examined the expression of both genes by whole-mount in situ hybridization between the four-cell stage and 4 days postfertilization (dpf) and found that both genes are expressed ubiquitously during early development with later restriction to regions of the head and anterior central nervous system (Fig. 2 *A1–A7* and *B1–B7*, and Fig. S2 *C1–C7* and *D1–D7*). Notably, at 48 h postfertilization (hpf) and 3 dpf, both genes are expressed in the heart (Fig. 2 *A4*, *B4*, *A6*, and *B6*, and Fig. S2 *C5*, *C6*, *D5*, and *D6*) and in the dorsal vessel (Fig. 2 *A3*, *B3*, *A5*, and *B5*, and Fig. S2 *C7* and *D7*). RT-PCR using RNA from wild-type 24-, 72-, and 84-hpf whole embryos or 3-dpf Tg(kdrl:GRCFP)zn1 GFP-positive sorted cells confirmed ex-

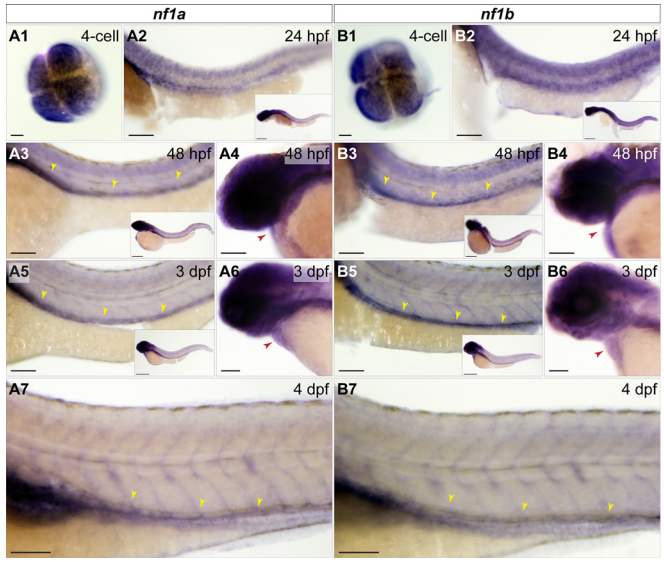

Fig. 2. *nf1a* and *nf1b* are expressed maternally and in the developing zebrafish cardiovascular system. Whole-mount in situ hybridization for *nf1a* and *nf1b* at the four-cell stage, 24 hpf, 48 hpf, 3 dpf, and 4 dpf. (*A1* and *B1*) At the four-cell stage, *nf1a* and *nf1b* are expressed throughout the animal pole of the developing embryo. (*A2* and *B2*) Both genes are expressed broadly at 24 hpf (*Inset*), with strong expression along the spinal cord. (*A3* and *B3*) At 48 hpf, expression of *nf1a* and *nf1b* is noted in the head and regions of the anterior trunk (*Inset*). Spinal cord expression of both genes persists, and positive staining is observed along the dorsal vessel for *nf1a* and *nf1b*. (*A4* and *B4*) Cardiac expression for both genes is observed at 48 hpf. (*A5* and *B5*) Expression of *nf1a* and *nf1b* become progressively restricted to regions of the head at 3 dpf (*Insets*). *nf1a* and *nf1b* expression along the dorsal vessel (*A5* and *B5*) and in the embryonic heart (*A6* and *B6*) persist at 3 dpf. (*A7* and *B7*) At 4 dpf, robust vascular staining is apparent for *nf1a* and *nf1b*. (Scale bars: 25 μm; 100 μm for insets.)

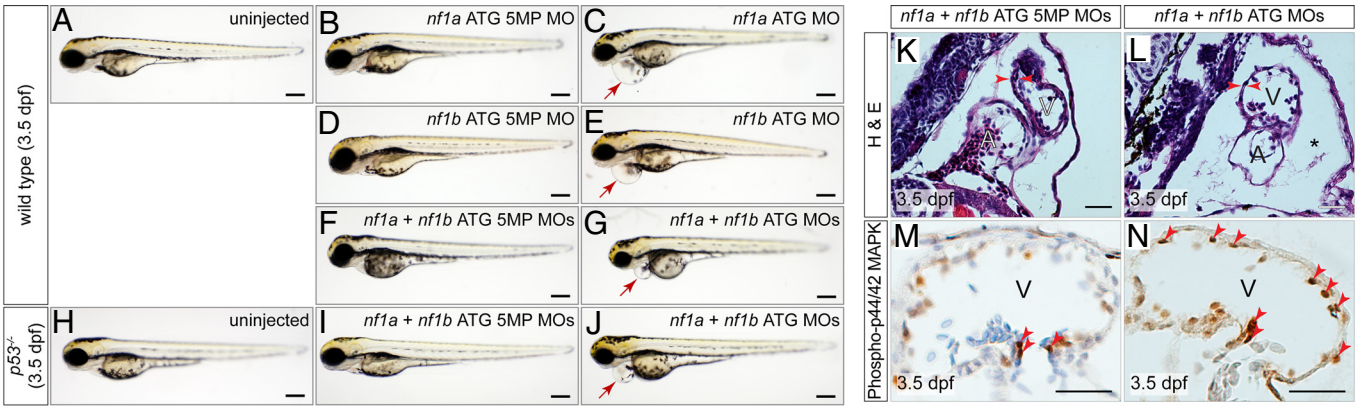

Fig. 3. MO knockdown of *nf1a*, *nf1b*, or both together results in pericardial effusions at 3.5 dpf and increased phospho-p44/42 MAPK in cardiac tissue. Analysis of 3.5-dpf wild-type embryos (*A*) or embryos injected with *nf1a* ATG 5-mispair (5MP) MO (*B*), *nf1b* ATG 5MP MO (*D*), or *nf1a* + *nf1b* ATG 5MP MO (*F*) reveal no apparent defects in gross morphology. Treatment with *nf1a* ATG MO (*C*), *nf1b* ATG MO (*E*), or a combination of both (*G*), however, results in a dilation of the pericardial space. (*H–J*) Injection of $p53^{-/-}$ embryos with *nf1a* + *nf1b* ATG MO results in a gross dilation of the pericardial space (*J*), whereas uninjected (*H*) and *nf1a* + *nf1b* ATG 5MP MO-injected $p53^{-/-}$ embryos (*I*) appear normal. (Scale bars: 0.25 mm.) (*K* and *L*) Transverse sections of 3.5-dpf *nf1a*/*nf1b* combined morphant embryos reveals a thinning of the ventricular myocardium and pericardial effusion (*) when compared with controls (A, atrium; V, ventricle). (*M* and *N*) Immunohistochemical analysis of transverse sections of 3.5-dpf *nf1a*/*nf1b* combined morphant embryos reveals an increase in the ratio of phospho-p44/42 MAPK-positive cardiac cells (arrows) to the total number of cardiac cells when compared with controls. (Scale bars: 25 μm.)

pression, particularly in the vascular endothelium (Fig. S2 *B–G*), whereas RNA from one-cell embryos indicate that both genes are expressed maternally (Fig. S2*B*). Queries of an expression database generated from sorted endothelial cells from Tg(fli1:egfp)y1 zebrafish identifies *nf1a* and *nf1b* in both GFP+ and GFP− cell populations, consistent with the expression of these genes in vascular endothelium (34).

Morpholino Knockdown of *nf1a* and *nf1b*. We used morpholino antisense oligonucleotides (MOs) to inhibit expression of *nf1a* and *nf1b* at early stages of development. Effectiveness of gene knockdown by translation blocking MO was confirmed by Western blot analysis (Fig. S3*A*). The ability of neurofibromin to function as a Ras-GAP, thereby down-regulating levels of active GTP-bound Ras, can result in decreased phosphorylation of downstream effectors, including Erk/MAPK. Western blots of 3.5-dpf whole-embryo extracts derived from *nf1a*, *nf1b*, or *nf1a*/*nf1b* morphants revealed a marked up-regulation of phospho-Erk in knockdown tissue, whereas levels of total Erk were unchanged (Fig. S3*B*). Efficacy of splice-blocking MOs was assessed by RT- and quantitative PCR using RNA collected from 24-hpf embryos (Fig. S3 *C–G*).

The phenotypes produced by MO treatment were compared in a blinded fashion to embryos injected with control MOs. We observed a marked increase in the intensity and domain of expression of glial fibrillary acidic protein (*GFAP*), a marker of Schwann and glial cells, by whole-mount in situ hybridization (Fig. S4). This finding is consistent with the increase in neural crest-derived tissue in $Nf1^{-/-}$ mice and the presence of neural crest-derived tumors in NF1 patients. We also examined the expression of myelin basic protein (*mbp*), sex-determining region Y-box 10 (*sox10*), forkhead box d3 (*foxd3*), and *crestin*, but did not observe changes. Therefore, the alterations observed in *nf1a* and *nf1b* morphant embryos appear to be restricted to the Schwann-glial lineages in the neural compartment.

Morpholino Knockdown of *nf1a* and *nf1b* Results in Cardiovascular Defects. *nf1a* and *nf1b* morphant embryos displayed gross abnormalities of cardiovascular development appreciable to the blinded observer by 48 hpf. Frequently, blood was seen to move back and forth from atrium to ventricle in morphants, suggesting a malfunctioning atrioventricular valve (Movies S1 and S2). At the resolution afforded to us by histological analysis, we observed no readily apparent structural defects in the atrioventricular valves of morphants despite the observed functional deficits (Fig. S5). In addition, we observed pooling of blood in the common cardinal vein and a paucity of blood flow along the dorsal aorta and posterior cardinal vein. Valvular insufficiency and reduced blood flow were not seen in control morphants or wild-type embryos (Movie S3). Overall development of the embryos was relatively preserved through the first 3 days despite these cardiac defects. Histological analysis revealed a thinned ventricular myocardium and large pericardial effusions in MO-treated embryos (Fig. 3 *K* and *L*, and Fig. S6 *A*, *B*, *F*, and *G*). Immunohistochemical analysis of 3.5-dpf *nf1a*, *nf1b*, and *nf1a*/*nf1b* morphant zebrafish also reveals increases in phospho-Erk staining (Fig. 3 *M* and *N*, and Fig. S6 *C–E* and *H–K*). Gross morphological analysis showed an increased incidence of pericardial effusions beginning at 48 hpf, reflecting cardiac dysfunction, in *nf1a* and *nf1b* morhpants when compared with controls (Fig. 3 *A–G*, and Fig. S6 *L* and *M*). Nonspecific toxicity arising from MO exposure as a cause of the observed cardiovascular defects was unlikely because unrelated control or scrambled MOs failed to produce similar levels of abnormalities, defects were observed even at low doses of specific MOs, and similar defects were observed with several unrelated but specific MOs directed against *nf1a* and *nf1b*. In addition, injection of specific MOs in *p53* mutant embryos also produced similar cardiovascular defects (Fig. 3 *H–J*), and off-target effects due to MO exposure are known to be partially mediated through *p53* activation (35). Defects in cardiac valve morphogenesis and a thinning of the ventricular myocardium are also seen in $Nf1^{-/-}$ murine embryos.

We performed knockdown experiments using zebrafish embryos in which endothelial cells are marked by expression of a cytoplasmic enhanced green fluorescent protein (GFP) to allow for a more detailed analysis of vascular development. Dramatic abnormalities of vascular patterning in the intersomitic vessels of morphant embryos were seen at 48 and 72 hpf (Fig. 4). In *nf1a* MO-treated embryos, the leading edge of the sprouting vessels displayed claw-like projections at 48 hpf (Fig. 4*C*) and failed to pattern normally such that the dorsal longitudinal anastomotic vessel (DLAV) did not form or developed in a rudimentary fashion (Fig. 4*F*). This occurred in embryos that were otherwise normal in overall size and maturity. These defects were also noted in *nf1a*/*nf1b* compound morphants, and were present but

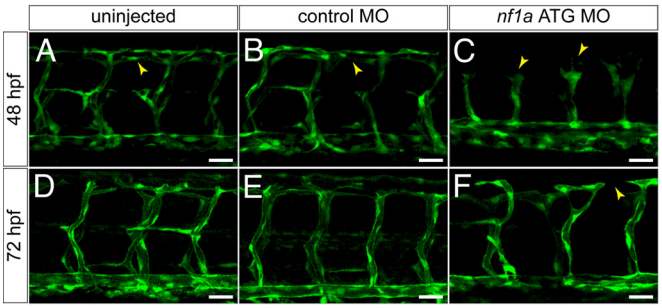

Fig. 4. MO knockdown of *nf1a* results in vascular patterning defects at 48 and 72 hpf. (*A–C*) At 48 hpf, *nf1a* ATG MO-treated Tg(fli:egfp)y1 (endothelial-specific GFP transgenic) zebrafish embryos display gross defects in vascular development compared with control MO-treated or uninjected samples. Morphant embryos (*C*) display abnormal claw-like projections at the leading edge of the developing intersomitic vessels and fail to develop the dorsal longitudinal anastomotic vessel (DLAV) present in both control MO-treated (*B*) and uninjected (*A*) samples. (*D–F*) At 72 hpf, *nf1a* ATG morphant embryos display only rudimentary DLAVs and a general disorganization of the trunk vasculature (*F*) when compared with control MO-treated (*E*) or uninjected (*D*) embryos. (Scale bars: 25 μm.)

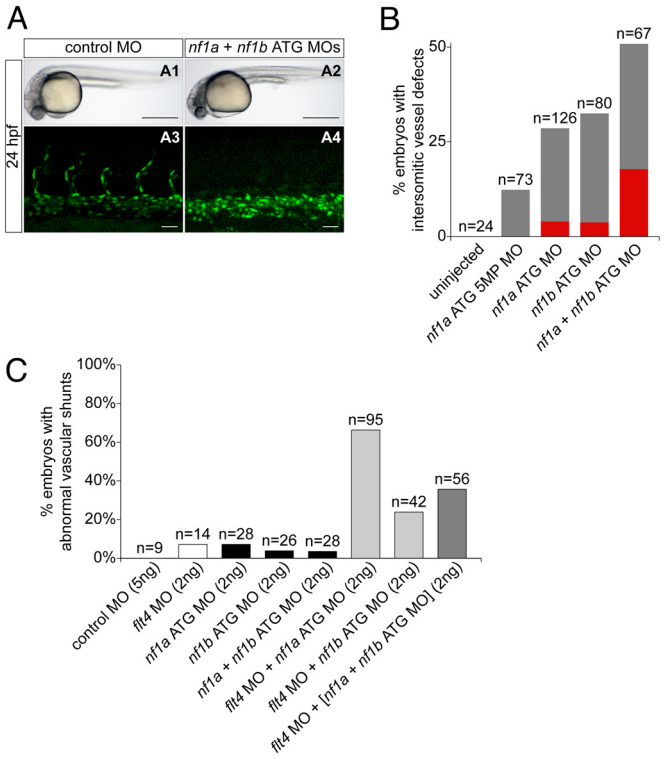

Fig. 5. MO knockdown of *nf1a*, *nf1b*, or both together result in vascular defects at 24 at 48 hpf. (*A* and *B*) Analysis and quantification of vascular defects at 24 hpf in uninjected and morphant Tg(fli:negfp)y7 (endothelial-specific nuclear GFP transgenic) zebrafish embryos. Control MO- (*A1*) and combined *nf1a*/*nf1b* MO-treated (*A2*) zebrafish embryos appear similar by gross morphological analysis at 24 hpf. (Scale bars: 500 μm.) Development of intersomitic vessels is deficient at 24 hpf in *nf1a*/*nf1b* combined morphants (*A4*) when compared with controls (*A3*). (Scale bars: 25 μm.) (*B*) Intersomitic vessel formation between somites 17–30 at 24 hpf was scored as absent (red), intermediate (gray), or normal following administration of 2 ng of the indicated MO(s). (*C*) MO-mediated knockdown of *flt4*, providing a sensitized background for the detection of vascular defects, was combined with *nf1a*, *nf1b*, and *nf1a* + *nf1b* ATG MO knockdown. Twenty-four to 85% of combined *flt4*/(*nf1a*, *nf1b*, *nf1a* + *nf1b*) MO-treated embryos display abnormal vascular shunts compared with 3–8% of individual *flt4*, *nf1a*, *nf1b*, or *nf1a* + *nf1b* MO-treated embryos.

less severe in *nf1b* morphants. Vascular patterning defects did not appear to correlate directly with cardiac defects, as we observed embryos with vascular abnormalities that did not display pericardial effusion or valvular insufficiency as assessed by a to-and-fro movement of blood within the heart (36). Blood flow within the dorsal aorta and posterior cardinal vein appeared intact in these embryos (Movie S4).

At 24 hpf, analysis using zebrafish embryos expressing a nuclear-localized GFP in endothelial cells indicated that morphants displayed a complete (Fig. 5*A4*) or partial absence of intersomitic vessels emanating from the dorsal aorta when compared with stage-matched controls (Fig. 5*A3*). Overall morphology of morphant and control embryos appeared equivalent (Fig. 5 *A1* and *A2*), ruling out nonspecific developmental delay. These defects were apparent following MO-mediated knockdown of *nf1a* or *nf1b*, whereas knockdown of both together had an additive effect (Fig. 5*B*). The small percentage of embryos with defects produced by the 5MP MO may have been due to low-level knockdown of *nf1a*. Again, similar defects were observed with several unrelated but specific MOs directed against *nf1a* and *nf1b* (Fig. S7*A*). Our analysis of morphant embryos at 24 hpf also revealed a caudal vessel defect. Morphant embryos displayed a cystic expansion in the region of the caudal vein and exhibited inappropriate anastomoses between the caudal vein and artery (Fig. S7 *D2–D4* and Movie S5) when compared with controls (Fig. S7D1). Identity of the expanded tissue as vascular was confirmed by expression of GFP (Fig. S7 *D6–D8*) and the observation of a pooling of red blood cells in the expanded region (Movie S5). This defect was present following knockdown of *nf1a*, *nf1b*, or both together (Fig. S7 *C* and *D*).

Additional confirmation of the role of *nf1a*/*nf1b* in vascular development derives from studies using a genetic background sensitized to vascular insult. Previous studies used MOs directed against *flt4*, the zebrafish VEGF receptor-3 orthologue, to investigate genetic interactions during zebrafish artery development (37). Additionally, *flt4* morphant zebrafish embryos display variable defects in segmental artery formation reminiscent of those identified in our *nf1a*/*nf1b* morphants. Endothelial-GFP expressing zebrafish embryos were injected with *flt4* MO alone and in combination with a MO directed against *nf1a*, *nf1b*, or a combination of both. At low MO doses, 85% of *flt4*/*nf1a*, 24% of *flt4*/*nf1b*, and 36% of *flt4*/*nf1a* + *nf1b* compound morphants displayed abnormal vascular shunts at 48 hpf compared with only 3–8% of individual *flt4*, *nf1a*, or *nf1b* morphants (Fig. 5*C*, Fig. S7*B*, and Movie S6). This defect was not apparent in controls (Movie S7). The shunts occur between the dorsal aorta and the dorsal longitudinal anastomotic vessel with retrograde flow through segmental arteries back into the dorsal aorta or through intersegmental veins into the posterior cardinal vein. In some cases, there were interruptions of the dorsal aorta.

Vascular Patterning Defects in Mouse Embryos Lacking *Nf1*. Although cardiac defects have been reported in mouse embryos lacking *Nf1*, a phenotype that has been attributed to a role for neurofibromin in endothelium (11), abnormalities in vascular patterning have not been previously identified. $Nf1^{-/-}$ mice succumb during midgestation and exhibit significant peripheral hemorrhage that has been hypothesized to be secondary to the intracardiac defects, although similar hemorrhage is not a common feature of mouse embryos with congenital heart disease. In light of our observation of peripheral vascular patterning defects in *nf1* morphant zebrafish embryos, we reevaluated murine *Nf1* knockouts by whole-mount platelet/endothelial cell adhesion molecule-1 (*PECAM-1*) staining to visualize endothelium at E10.5–E11.5 time points before the development of overt cardiac failure or significant endocardial cushion defects. Although no

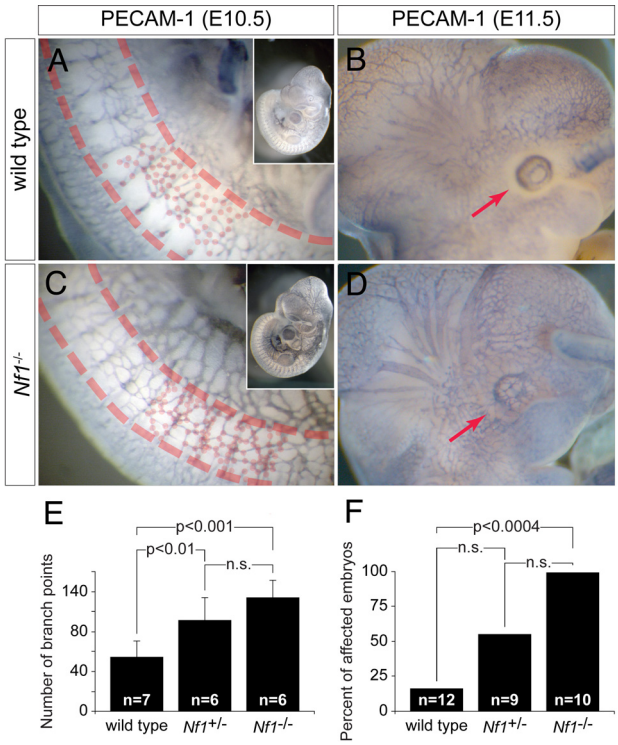

Fig. 6. *Nf1*$^{-/-}$ mouse embryos display defects in vascular patterning. (*A* and *C*) Whole-mount PECAM-1 staining of E10.5 wild-type (*A*) and *Nf1*$^{-/-}$ (*C*) mouse embryos reveals abnormal vascular patterning in *Nf1*$^{-/-}$ embryos, with an increased number of vessels and branching (dots at branch points) particularly evident in the somites (between dashed lines). Low-magnification insets show an overall increase in vascular staining in *Nf1*$^{-/-}$ embryos. (*E*) Quantification of vessel branch points over four somites immediately rostral to the anterior limb buds at E10.5 shows a significant increase in *Nf1*$^{+/-}$ and *Nf1*$^{-/-}$ embryos compared with wild type (±SD). (*B* and *D*) Similar staining of stage-matched littermates at E11.5 reveals loss of the normal avascular zone around the developing eye (*D*) in *Nf1*$^{-/-}$ embryos compared with wild type (*B*). (*F*) Quantification of abnormal eye vasculature shows a significant increase in the number of affected *Nf1*$^{-/-}$ embryos compared with wild types ($P < 0.004$).

overt differences were appreciated in E11.5 yolk sacs (Fig. S8), we identified vascular abnormalities in embryos, including an increase in overall vascularity and a failure of the primitive vascular plexuses in the somitic region and head to remodel as seen in wild-type embryos (Fig. 6). These findings suggest that peripheral hemorrhage commonly noted on *Nf1*$^{-/-}$ mouse embryos may be related to an intrinsic vascular defect similar to that identified in MO knockdown zebrafish.

Discussion

We report the identification and initial characterization of the zebrafish orthologues of the human neurofibromatosis gene *NF1*. The two zebrafish *nf1* genes likely arose from a genome duplication event and are highly related to one another in structure, sequence, and expression pattern through early development. MO-mediated knockdown of either gene alone results in developmental defects involving cardiac and neural crest structures that are even more prominent when both genes are knocked down in concert, suggesting partial functional redundancy. Interestingly, the entire spectrum of cardiovascular defects we have identified, including pericardial effusions and functional valve abnormalities, segmental vessel defects, and aberrant arteriovenous shunts, are greater with knockdown of the *nf1a* orthologue compared with *nf1b*, suggesting that *nf1a* may play a more prominent role in cardiovascular development.

Nf1$^{-/-}$ mice die during midgestation as a result of severe cardiac failure, and display gross cardiovascular and neural crest defects. Closer examination of these *Nf1*-defcient mice reveals hyperproliferative endocardial cushions, the precursors of the cardiac valves, which have been shown to result from a cell-autonomous role for *Nf1* in endothelial cells (11). Here, we show that zebrafish embryos also display cardiovascular and neural abnormalities following transient knockdown of the orthologous *nf1* genes. These defects resemble those seen in mouse models, including the presence of pericardial effusions, thinned myocardium, abnormal cardiac valves, and an increase in Schwann-glial derivatives.

Importantly, the generation of a new vertebrate model of NF1 allowed us to identify a previously unrecognized role for neurofibromin in vascular patterning during early zebrafish and murine development. The ability to distinguish a primary vascular defect from a phenotype resulting secondary to cardiac failure is possible in zebrafish because early vascular development does not require an intact circulation, and adequate oxygenation is achieved via passive diffusion (38). In mice, this distinction is much more difficult to define, emphasizing one of the advantages of developing a zebrafish model of NF1. It is worth noting that the degree of peripheral hemorrhage noted in *Nf1* knockout embryos is unusual for mouse models of congenital heart disease and is not seen in embryos with double-outlet right ventricle, truncus arteriosus, or atrioventricular canal defects despite pericardial effusions indicating heart failure (39). We hypothesize that a peripheral vascular defect produced by endothelial dysfunction in *Nf1*-deficient mouse embryos accounts for the observed degree of hemorrhage. Though the complexity and severity of vascular patterning defects in mouse and zebrafish embryos lacking neurofibromin are distinct, we suggest that they are highly likely to be related, and there is precedent for similar differences in the vascular manifestation of genetic mutations in fish and mice (40, 41).

Vascular patterning defects represent a well-recognized component of the pleiotropic spectrum of NF1 disease phenotypes in affected individuals (3). NF1 patients often exhibit a characteristic vascular lesion known as moyamoya, a name that derives from its appearance as a puff of smoke on computed tomography scans of the head due to abnormal small-vessel patterning in the brain (42, 43). Other vascular defects, including hypertension and renal artery stenosis, have also been documented (3). Neurofibromin has been shown to modulate the activity of Ras proto-oncogenes through its GAP-related domain (GRD), and multiple lines of evidence support a role for Ras signaling in normal vascular patterning and development. For example, mouse embryos deficient for p120 GAP activity display vascular defects such as abnormalities in endothelial cell organization (44). In addition, mutations in *RASA1*, the gene encoding p120 GAP, are associated with vascular anomalies in affected individuals (45, 46). Experiments in chicken and mouse endothelial tissues have identified a role for H-Ras in angiogenesis and vascular permeability (47). Studies in zebrafish also support a role for Ras signaling in vascular development; MO knockdown of *k-ras* or overexpression of a dominant negative mutant of *k-ras* both result in defective vascular development (48). These data, taken together with our own, suggest a necessity for tight regulation of Ras signaling in normal vascular development. The *flt4*/(*nf1a*, *nf1b*, *nf1a* + *nf1b*) vascular shunting phenotype represents an inappropriate arteriovenous malformation, which is also present in the embryos with cystic expansion of the dorsal vein. Other vascular patterning defects observed in the *nf1a*/*nf1b* morphants may represent distinct functions of neurofibromin in the vasculature, or may be related by common underlying mechanisms. The genetic interaction between *nf1a*/*nf1b* and *flt4* that we show suggests that these molecules may function in a

DEVELOPMENTAL BIOLOGY

common molecular pathway, although alternative interpretations cannot be ruled out.

In an effort to determine the degree to which neurofibromin function can be ascribed to its activity as a Ras-GAP, we have previously generated a mouse model in which the isolated neurofibromin GRD is expressed in a tissue-restricted manner upon Cre-mediated activation (20). These studies have shown that reconstitution of the neurofibromin GRD in endothelial cells of *Nf1*$^{-/-}$ mice is sufficient to rescue cardiac development and midgestational lethality. The resulting mice, however, are abnormal and succumb in the early postnatal period. Analysis of these animals reveals massive overgrowth of peripheral nervous tissues that mimic those of the neural crest-specific *Nf1*-deleted mice. This finding strongly suggests that additional domains outside the GRD are important for neural crest growth and homeostasis. Our development of a zebrafish model of NF1 will be particularly useful for examining the potential activities of these domains through in vivo structure-function analyses. Enhancer and suppressor screens may identify signaling pathways, in addition to the Ras/MAPK and mTOR pathways, that impact disease progression. In addition, high-throughput small-molecule screens will allow for the rapid identification of compounds with the potential for modifying NF1 disease phenotypes. The generation of stable mutant lines for *nf1a* and *nf1b* serve as a necessary prerequisite to pursue these exciting possibilities.

Materials and Methods

Morpholino Injections. Morpholino oligonucleotides (Gene Tools) corresponding to *nf1a*, *nf1b*, *flt4*, and associated controls were dissolved in water and supplemented with 0.1% vol/vol phenol red. One-cell zebrafish embryos were injected with ≈1 nL of the appropriate MO solution(s). MO sequences were as follows: *nf1a* ATG MO 5′-GGCTTGTGCGCCGCCATGCTCAGGG, *nf1a* ATG 5MP MO (*nf1a* ATG 5-mispair control MO) 5′-GGCTTCTGCCCCGGCATGGTCACGC, *nf1b* ATG MO 5′-CCGCTCACGCCGATAGTGATGAAGA, *nf1b* ATG 5MP MO 5′-CCCCTCAGGCCCATAGTCATCAAGA, *nf1a* SB MO 5′-GTCCAAGTAGTGTTTTCCTTACCTG, *nf1a* SB 5MP MO 5′-GTCCAACTACTCTTTTGCTTAGCTG, *nf1b* SB MO 5′-CTCAGTATTTATCTGCACCTGGTGG, *nf1b* SB 5MP MO 5′-CTGAGTATATATGTGCAGCTGCTGG, *flt4* MO (37), and standard control MO 5′-CCTCTTACCTCAGTTACAATTTATA.

Additional information is available in *SI Materials and Methods*.

ACKNOWLEDGMENTS. We thank Jie He (University of Pennsylvania CDB Zebrafish Core) and Nicole Antonucci for assistance with animal husbandry, Andrea Stout (University of Pennsylvania CDB/CVI Microscopy Core) for assistance with microscopy, and Michael Pack and Mary Mullins for helpful discussions and reagents. This work was supported by National Institutes of Health Grants R01-HL062974 (to J.A.E.) and K08-HL075179 (to F.A.I.) and Department of Defense Grant NF050175 (to J.A.E. and A.T.L.). A.P. was supported by a fellowship from the Sarnoff Cardiovascular Research Foundation, and J.-S.L. was supported by a Young Investigator Award from the Children's Tumor Foundation.

1. Ferner RE, et al. (2007) Guidelines for the diagnosis and management of individuals with neurofibromatosis 1. *J Med Genet* 44(2):81–88.
2. Viskochil D (2002) Genetics of neurofibromatosis 1 and the NF1 gene. *J Child Neurol* 17(8):562–570; discussion: 571–562, 646–551.
3. Friedman JM, et al. (2002) Cardiovascular disease in neurofibromatosis 1: Report of the NF1 Cardiovascular Task Force. *Genet Med* 4(3):105–111.
4. Cichowski K, Jacks T (2001) NF1 tumor suppressor gene function: Narrowing the GAP. *Cell* 104(4):593–604.
5. Guo HF, The I, Hannan F, Bernards A, Zhong Y (1997) Requirement of Drosophila NF1 for activation of adenylyl cyclase by PACAP38-like neuropeptides. *Science* 276(5313):795–798.
6. The I, et al. (1997) Rescue of a Drosophila NF1 mutant phenotype by protein kinase A. *Science* 276(5313):791–794.
7. Tong J, Hannan F, Zhu Y, Bernards A, Zhong Y (2002) Neurofibromin regulates G protein-stimulated adenylyl cyclase activity. *Nat Neurosci* 5(2):95–96.
8. Hegedus B, et al. (2007) Neurofibromatosis-1 regulates neuronal and glial cell differentiation from neuroglial progenitors in vivo by both cAMP- and Ras-dependent mechanisms. *Cell Stem Cell* 1(4):443–457.
9. Xu H, Gutmann DH (1997) Mutations in the GAP-related domain impair the ability of neurofibromin to associate with microtubules. *Brain Res* 759(1):149–152.
10. Hsueh Y, Roberts AM, Volta M, Sheng M, Roberts RG (2001) Bipartite interaction between neurofibromatosis type I protein (neurofibromin) and syndecan transmembrane heparan sulfate proteoglycans. *J Neurosci* 21(11):3764–3770.
11. Gitler AD, et al. (2003) Nf1 has an essential role in endothelial cells. *Nat Genet* 33(1):75–79.
12. Brannan CI, et al. (1994) Targeted disruption of the neurofibromatosis type-1 gene leads to developmental abnormalities in heart and various neural crest-derived tissues. *Genes Dev* 8(9):1019–1029.
13. Jacks T, et al. (1994) Tumour predisposition in mice heterozygous for a targeted mutation in Nf1. *Nat Genet* 7(3):353–361.
14. Cichowski K, et al. (1999) Mouse models of tumor development in neurofibromatosis type 1. *Science* 286(5447):2172–2176.
15. Vogel KS, et al. (1999) Mouse tumor model for neurofibromatosis type 1. *Science* 286(5447):2176–2179.
16. Reilly KM, Loisel DA, Bronson RT, McLaughlin ME, Jacks T (2000) Nf1;Trp53 mutant mice develop glioblastoma with evidence of strain-specific effects. *Nat Genet* 26(1):109–113.
17. Costa RM, et al. (2001) Learning deficits, but normal development and tumor predisposition, in mice lacking exon 23a of Nf1. *Nat Genet* 27(4):399–405.
18. Zhu Y, et al. (2001) Ablation of NF1 function in neurons induces abnormal development of cerebral cortex and reactive gliosis in the brain. *Genes Dev* 15(7):859–876.
19. Zhu Y, Ghosh P, Charnay P, Burns DK, Parada LF (2002) Neurofibromas in NF1: Schwann cell origin and role of tumor environment. *Science* 296(5569):920–922.
20. Ismat FA, Xu J, Lu MM, Epstein JA (2006) The neurofibromin GAP-related domain rescues endothelial but not neural crest development in Nf1 mice. *J Clin Invest* 116(9):2378–2384.
21. Joseph NM, et al. (2008) The loss of Nf1 transiently promotes self-renewal but not tumorigenesis by neural crest stem cells. *Cancer Cell* 13(2):129–140.
22. Wu J, et al. (2008) Plexiform and dermal neurofibromas and pigmentation are caused by Nf1 loss in desert hedgehog-expressing cells. *Cancer Cell* 13(2):105–116.
23. Zheng H, et al. (2008) Induction of abnormal proliferation by nonmyelinating Schwann cells triggers neurofibroma formation. *Cancer Cell* 13(2):117–128.
24. Silva AJ, et al. (1997) A mouse model for the learning and memory deficits associated with neurofibromatosis type I. *Nat Genet* 15(3):281–284.
25. Costa RM, et al. (2002) Mechanism for the learning deficits in a mouse model of neurofibromatosis type 1. *Nature* 415(6871):526–530.
26. Li H, Velasco-Miguel S, Vass WC, Parada LF, DeClue JE (2002) Epidermal growth factor receptor signaling pathways are associated with tumorigenesis in the Nf1:p53 mouse tumor model. *Cancer Res* 62(15):4507–4513.
27. Zhu Y, et al. (2005) Early inactivation of p53 tumor suppressor gene cooperating with NF1 loss induces malignant astrocytoma. *Cancer Cell* 8(2):119–130.
28. Le L, Parada L (2007) Tumor microenvironment and neurofibromatosis type I: Connecting the GAPs. *Oncogene* 26(32):4609–4616.
29. Side LE, et al. (1998) Mutations of the NF1 gene in children with juvenile myelomonocytic leukemia without clinical evidence of neurofibromatosis, type 1. *Blood* 92(1):267–272.
30. Le DT, et al. (2004) Somatic inactivation of Nf1 in hematopoietic cells results in a progressive myeloproliferative disorder. *Blood* 103(11):4243–4250.
31. Gitler A, et al. (2004) Tie2-Cre-induced inactivation of a conditional mutant Nf1 allele in mouse results in a myeloproliferative disorder that models juvenile myelomonocytic leukemia. *Pediatr Res* 55(4):581–584.
32. Yang FC, et al. (2008) Nf1-dependent tumors require a microenvironment containing Nf1+/− and c-kit-dependent bone marrow. *Cell* 135(3):437–448.
33. Amores A, et al. (1998) Zebrafish hox clusters and vertebrate genome evolution. *Science* 282(5394):1711–1714.
34. Covassin L, et al. (2006) Global analysis of hematopoietic and vascular endothelial gene expression by tissue specific microarray profiling in zebrafish. *Dev Biol* 299(2):551–562.
35. Robu ME, et al. (2007) p53 activation by knockdown technologies. *PLoS Genet* 3(5):e78.
36. Isogai S, Lawson ND, Torrealday S, Horiguchi M, Weinstein BM (2003) Angiogenic network formation in the developing vertebrate trunk. *Development* 130(21):5281–5290.
37. Covassin LD, Villefranc JA, Kacergis MC, Weinstein BM, Lawson ND (2006) Distinct genetic interactions between multiple Vegf receptors are required for development of different blood vessel types in zebrafish. *Proc Natl Acad Sci USA* 103(17):6554–6559.
38. Vogel AM, Weinstein BM (2000) Studying vascular development in the zebrafish. *Trends Cardiovasc Med* 10(8):352–360.
39. Gruber PJ, Epstein JA (2004) Development gone awry: Congenital heart disease. *Circ Res* 94(3):273–283.
40. Gitler A (2004) PlexinD1 and semaphorin signaling are required in endothelial cells for cardiovascular development. *Dev Cell* 7(1):107–116.
41. Torresvazquez J (2004) Semaphorin-plexin signaling guides patterning of the developing vasculature. *Dev Cell* 7(1):117–123.
42. Norton KK, Xu J, Gutmann DH (1995) Expression of the neurofibromatosis I gene product, neurofibromin, in blood vessel endothelial cells and smooth muscle. *Neurobiol Dis* 2(1):13–21.
43. Cairns AG, North KN (2008) Cerebrovascular dysplasia in neurofibromatosis type 1. *J Neurol Neurosurg Psychiatr* 79(10):1165–1170.
44. Henkemeyer M, et al. (1995) Vascular system defects and neuronal apoptosis in mice lacking ras GTPase-activating protein. *Nature* 377(6551):695–701.
45. Eerola I, et al. (2003) Capillary malformation–arteriovenous malformation, a new clinical and genetic disorder caused by RASA1 mutations. *Am J Hum Genet* 73(6):1240–1249.
46. Revencu N, et al. (2008) Parkes Weber syndrome, vein of Galen aneurysmal malformation, and other fast-flow vascular anomalies are caused by RASA1 mutations. *Hum Mutat* 29(7):959–965.
47. Serban D, Leng J, Cheresh D (2008) H-ras regulates angiogenesis and vascular permeability by activation of distinct downstream effectors. *Circ Res* 102(11):1350–1358.
48. Liu L, Zhu S, Gong Z, Low BC (2008) K-ras/PI3K-Akt signaling is essential for zebrafish hematopoiesis and angiogenesis. *PLoS ONE* 3(8):e2850.